Journal of Luminescence 294 (2026) 121846

Contents lists available at ScienceDirect

Journal of Luminescence

journal homepage: www.elsevier.com/locate/jlumin

Full Length Article

Thermoluminescence properties and trap kinetics of $SmCa_4(BO_3)_3$ phosphor

E. Aymila Cin [a], K. Bulcar [b], Abeer S. Altowyan [c], M.B. Coban [d,e], U.H. Kaynar [f], H. Muzaffer Sagban [g], Jabir Hakami [h], M. Topaksu [i], N. Can [h,*]

[a] Bakırcay University, Graduate School of Natural and Applied Sciences, Menemen, Izmir, Turkiye
[b] Igdir University, Vocational School of Health Services, Karaagac Campus, Igdir, 76000, Turkiye
[c] Department of Physics, College of Science, Princess Nourah Bint Abdulrahman University, P.O. Box 84428, Riyadh, 11671, Saudi Arabia
[d] Balikesir University, Faculty of Arts and Sciences, Department of Physics, Balikesir, Turkiye
[e] Balikesir University, Science and Technology Application and Research Center, Balikesir, Turkiye
[f] Bakircay University, Faculty of Engineering and Architecture, Department of Fundamental Sciences, Menemen, Izmir, Turkiye
[g] Istanbul Beykent University, Opticianry, Vocational School, Beylikduzu, İstanbul, Turkiye
[h] Jazan University, College of Science, Department of Physical Sciences, Physics Division, P.O. Box 114, Jazan, 45142, Kingdom of Saudi Arabia
[i] Physics Department, Cukurova University, Arts-Sciences Faculty, Adana, 01330, Turkiye

ARTICLE INFO

Keywords:
$SmCa_4O(BO_3)_3$ ceramic
Thermoluminescence
Trap kinetics
Anomalous time-dependent enhancement
Radiation dosimetry

ABSTRACT

Undoped $SmCa_4O(BO_3)_3$ (SCOB) phosphor was synthesized by a microwave-assisted sol–gel combustion method and confirmed as single-phase monoclinic by X-ray diffraction. Thermoluminescence (TL) was measured after β-irradiation up to 500 Gy at a linear heating rate of 2 °C/s between room temperature and 450 °C. The glow curve at 50 Gy shows two main peaks at about 80 °C and 240 °C; after optimized preheating at 180 °C for 10 s, a single dominant peak near 247 °C remains and is used for all further measurements. The main peak shows good reusability over repeated readouts and a wide dose–response range from ~1 to about 500 Gy without saturation. Kinetic analysis of this peak using variable heating rate, initial rise, and glow-curve deconvolution yields activation energies around 1.6–1.8 eV and frequency factors of $\sim 10^{14}$–10^{16} s^{-1}, indicating a thermally stable trapping level suitable for dosimetric applications.

1. Introduction

Thermoluminescence (TL) is a well-established phenomenon extensively employed in radiation dosimetry, defect characterization, and solid-state luminescence studies [1]. The process involves the trapping of charge carriers at metastable defect states during irradiation, followed by their thermal release, resulting in light emission. The temperature-dependent TL glow curve encodes valuable information on trap depth, recombination probability, and kinetic order, making TL a powerful tool for investigating charge carrier dynamics in insulating and semiconducting materials [2,3]. Borate-based compounds are attractive TL host materials due to their chemical stability and wide band gaps, which favor the formation of stable intrinsic and radiation-induced trapping centers [4–8].

Previous studies on multi-cation borates, including $K_7SrY_2(B_5O_{10})_3$ and rare-earth-containing calcium oxyborates such as $GdCa_4O(BO_3)_3$: Sm, have demonstrated that intrinsic defects and rare-earth ions significantly influence TL glow curve structure and kinetic parameters [9,10]. Rare-earth ions are frequently employed in borate matrices to tailor luminescent and kinetic properties. Among them, Sm^{3+} ions are of particular interest due to their sensitivity to the local crystal field and their interactions with defect-related trapping centers. In calcium-based borates, Sm^{3+} acts both as a luminescent center and as a trap-related center that modifies charge carrier capture and recombination processes [11–13]. Despite these advances, systematic TL studies focusing specifically on samarium-containing calcium oxyborate hosts remain relatively limited. Recent studies suggest that trapping centers in complex borates may involve defect interactions rather than isolated traps [14]. However, despite these findings, $SmCa_4O(BO_3)_3$ (SCOB) has not been systematically investigated in terms of its TL behavior. In particular, the nature of its trapping centers, their kinetic parameters, and the interaction between intrinsic and Sm-related defects remain unclear. A

* Corresponding author.
E-mail addresses: asaltowyan@pnu.edu.sa (A.S. Altowyan), ncan@jazanu.edu.sa (N. Can).

https://doi.org/10.1016/j.jlumin.2026.121846
Received 20 January 2026; Received in revised form 17 February 2026; Accepted 9 March 2026
Available online 11 March 2026

detailed TL study is therefore necessary to clarify the trapping mechanism and to evaluate the suitability of SCOB as a potential borate-based dosimetric material [15–17].

In this study, SCOB phosphors were synthesized by a sol–gel combustion method and structurally confirmed by X-ray diffraction. The TL properties induced by β-irradiation were characterized using initial rise, variable heating rate, computerized glow curve deconvolution, and T_m–T_{stop} protocol. These complementary methods were used to determine activation energies, frequency factors, and kinetic order of the main TL peak and to identify the dominant trapping centers responsible for the dosimetric response of SCOB.

2. Experimental

2.1. Preparation of SCOB phosphors

SCOB phosphor samples were synthesized using a microwave-assisted sol–gel combustion route, selected for its ability to provide homogeneous mixing of precursors and rapid formation of crystalline products. Analytical-grade samarium (III) oxide (Sm_2O_3, Sigma, Aldrich ≥99.9%), calcium nitrate tetrahydrate ($Ca(NO_3)_2{\cdot}4H_2O$, Sigma Aldrich ≥99.0%), and boric acid (H_3BO_3, Sigma Aldrich ≥99.5%) were used as starting materials without further purification. Prior to synthesis, Sm_2O_3 was converted into samarium nitrate by dissolving the oxide in dilute nitric acid under gentle heating until a clear solution was obtained. The resulting samarium nitrate solution was mixed with stoichiometric amounts of calcium nitrate and boric acid, corresponding to the nominal composition of SCOB. The precursors were dissolved in deionized water under continuous magnetic stirring to ensure complete homogenization. Urea and glycine were introduced as fuel agents to promote the combustion process and to facilitate uniform heat distribution during microwave irradiation. The solution was maintained at approximately 80 °C and stirred for about 1 h, leading to gradual evaporation of the solvent and the formation of a viscous gel. The gel was subsequently subjected to microwave irradiation at a power of 800 W for a duration of 2 min. During this stage, a rapid self-sustaining combustion reaction occurred, accompanied by the release of gaseous by-products, resulting in the formation of a voluminous white precursor powder. To improve crystallinity and remove residual organic species, the as-combusted product was annealed in air at 1000 °C for 4 h. After thermal treatment, fine white $SmCa_4O(BO_3)_3$ powders were obtained. The synthesized phosphors were allowed to cool naturally to room temperature and then stored in a desiccator to minimize moisture uptake prior to structural and thermoluminescence characterization.

2.2. TL measurements

TL measurements were performed using a *Lexsyg Smart TL/OSL reader* (Freiberg Instruments, Germany), housed at Bakircay University, and equipped with a built-in $^{90}Sr/^{90}Y$ beta source calibrated to deliver a nominal dose rate of ~1.436 Gy/s. Prior to each measurement, approximately 20 mg of the $SmCa_4O(BO_3)_3$ powder was gently ground and pressed into circular pellets of 6 mm diameter and an approximate thickness of ~0.5 mm using a manual hydraulic press. This ensured reproducible sample geometry and good thermal contact with the stainless-steel heater planchet during heating.

The irradiated samples were heated from room temperature up to 450 °C under a linear heating regime. A standard heating rate of 2 °C/s was used for initial glow curve acquisition. To investigate the influence of thermal ramping on trap dynamics and peak shapes, additional measurements were conducted at varied heating rates ranging from 0.1 °C/s to 5 °C/s. All experiments were conducted under continuous nitrogen flow to prevent surface oxidation and suppress spurious chemiluminescence signals.

Background subtraction was applied systematically to each glow curve using control data acquired from non-irradiated samples measured under identical conditions. Special care was taken to minimize premature trap depopulation: irradiated samples were stored in opaque containers and handled under red-light conditions until the point of measurement. To further enhance measurement reproducibility and reduce signal noise potentially caused by uneven particle packing, the powders were lightly homogenized in an agate mortar prior to pellet pressing.

This protocol allowed for precise characterization of TL features inherent to the SCOB matrix, forming a consistent basis for subsequent kinetic modeling and trap parameter analysis.

2.3. Methods of analysis

Thermoluminescence (TL) glow curves provide direct insight into the nature of trapping and recombination processes through their characteristic shape and temperature dependence. In order to extract reliable kinetic parameters associated with the charge traps in SCOB, a combination of complementary analytical techniques was employed. The kinetic analysis focused on the determination of activation energy (E), frequency factor (s), and kinetic order (b) using the Variable Heating Rate (VHR) method, T_m–T_{stop} analysis, computerized glow curve deconvolution (CGCD), and the initial rise (IR) method. Temperature lag correction was applied separately as a data correction procedure to improve the accuracy of peak temperature values prior to kinetic evaluation.

2.3.1. Variable heating rate (VHR) method

The VHR method, originally proposed by Hoogenstraaten [18], was applied to evaluate the activation energy and frequency factor of the dominant TL glow peaks. This method is based on the systematic shift of the glow peak maximum temperature (T_m) towards higher temperatures with increasing heating rate (β). For a given trapping level, the relationship between T_m and β can be expressed by the following equation [18,19].

$$ln\left(\frac{T_m^2}{\beta}\right) = \frac{E}{k_B T_m} + ln\left(\frac{E}{s k_B}\right) \quad (1)$$

where E is the activation energy, s is the frequency factor, k_B is the Boltzmann constant, and T_m is the peak temperature. A linear fit of $ln\left(\frac{T_m^2}{\beta}\right)$ versus $1/k_B T_m$ yields the activation energy from the slope, while the frequency factor is obtained from the intercept. The VHR method is particularly advantageous because it does not require prior assumptions regarding the order of kinetics and is well-suited for analyzing dominant peaks in complex glow curves.

2.3.2. Temperature lag correction

At higher heating rates, discrepancies may arise between the nominal sample temperature and the actual temperature of the phosphor due to thermal inertia, commonly referred to as temperature lag. To minimize systematic errors in the determination of kinetic parameters, a temperature lag correction was applied using the approach proposed by Kitis and Tuyn [20]. The corrected peak temperature was calculated using:

$$T_j = T_i - \left(\frac{T_2 - T_1}{ln(\beta_2/\beta_1)}\right) ln\left(\frac{\beta_i}{\beta_j}\right) \quad (2)$$

where T_i and T_j are the measured and corrected peak temperatures corresponding to heating rates β_i and β_j, respectively. T_1 and T_2 denote peak temperatures measured at low heating rates, where temperature lag effects are negligible. This correction ensures consistency in VHR analysis and improves the accuracy of activation energy and frequency factor determination.

2.3.3. T_m–T_{stop} method

The T_m–T_{stop} method was used to examine the structure of the TL glow curve and to evaluate the presence of overlapping components. In this approach, the sample is first heated to a selected stop temperature (T_{stop}), cooled to room temperature, and then reheated to record the residual TL glow curve. The maximum temperature (T_m) of the residual glow curve is plotted as a function of T_{stop}.

A plateau region in the T_m–T_{stop} plot is generally associated with a dominant discrete trapping level, whereas a gradual increase in T_m with T_{stop} suggests the contribution of distributed or closely spaced trap levels [21,22]. The method therefore provides qualitative insight into the complexity of the trap structure, while quantitative activation energies were determined independently using the initial rise method.

2.3.4. Initial rise (IR) method

The IR method, first proposed by Garlick and Gibson [23], is based on the analysis of the low-temperature rising edge of a TL glow peak, where the TL intensity increases exponentially with temperature. In this low-temperature region, the TL intensity follows an Arrhenius-type relationship, assuming that the frequency factor remains temperature independent.

The TL intensity in the initial rise region can be expressed as:

$$I = c\exp(-E/kT) \tag{3}$$

where c is a constant, E is the activation energy (trap depth), T is the absolute temperature, and k is the Boltzmann constant. A plot of $ln(I)$ versus $1/kT$ yields a straight line, and the slope of this line corresponds to the activation energy of the trap responsible for the TL glow peak.

2.3.5. Computerized glow curve deconvolution (CGCD)

To quantitatively resolve overlapping TL peaks and extract individual kinetic parameters, computerized glow curve deconvolution (CGCD) was performed using a general-order kinetic model developed by Gomez-Ros and Kitis [24]. The experimental glow curves were fitted by assuming a superposition of individual TL peaks, each described by a general-order kinetic equation:

$$I(T) = I_m \exp\left(\frac{E}{kT_m^2}(T-T_m)\right)\left[\frac{1}{b}+\frac{b-1}{b}\exp\left(\frac{E}{kT_m^2}(T-T_m)\right)\right]^{-\frac{b}{b-1}} \tag{4}$$

where I_m is the maximum TL intensity, E is the activation energy, T_m is the peak temperature, and b is the kinetic order. Once E, T_m, and b were obtained from the fitting procedure, the frequency factor s was calculated using [19]:

$$s = \frac{E}{k_B T_m^2}\exp\left(\frac{E}{k_B T_m}\right) \tag{5}$$

The quality of the deconvolution was evaluated using the figure of merit (FOM), defined as the normalized difference between the experimental and fitted glow curves [25,26]. FOM values below 5% were considered indicative of satisfactory agreement. The deconvolution analysis was carried out using the tgcd package implemented in the R statistical computing framework, which enables automated fitting based on general-order kinetics and provides robust handling of complex glow curve structures [27].

3. Results and discussions

3.1. Structural analysis

XRD analysis confirms that SCOB crystallizes in a monoclinic structure consistent with the reference data (Fig. 1). The refined lattice parameters were determined as a = 8.118 Å, b = 16.055 Å, c = 3.558 Å, β = 101.43°, with a unit cell volume of 457.31 Å^3. These values are in good agreement with reported crystallographic data, indicating successful phase formation (see Fig. 2).

The XRD pattern of SCOB was refined by the Rietveld method (Fig. 1b) using the monoclinic SCOB structural model (Ref. pattern code: 98-006-6369). The refinement shows good agreement between the observed and calculated profiles, with acceptable reliability factors (χ^2 = 2.16, R_p = 0.050, R_{wp} = 0.060, R_{exp} = 0.031). Within the

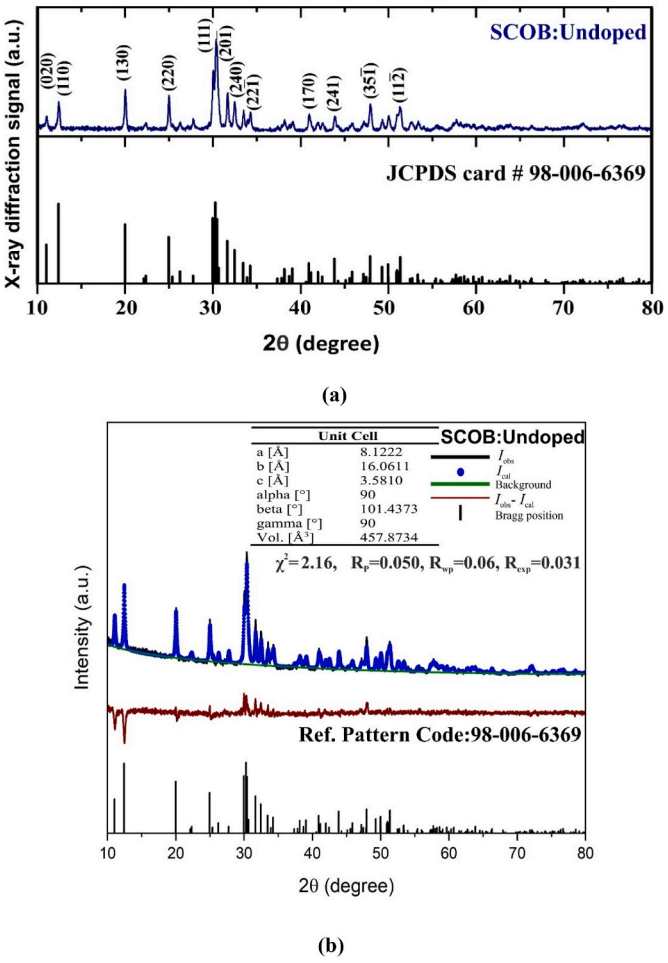

Fig. 1. (a) X-ray diffraction (XRD) pattern of (SCOB) phosphor synthesized by the microwave-assisted sol–gel combustion method. (b) Rietveld refinement of the X-ray diffraction pattern of SCOB phosphor using the monoclinic structural model.

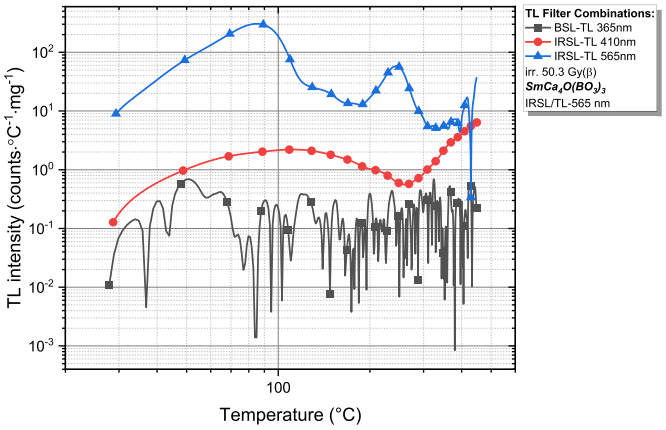

Fig. 2. TL glow curves of SCOB recorded after 50.3 Gy β-irradiation using IRSL/TL filters (365, 410, and 565 nm) on a log–log scale.

instrumental resolution, all significant reflections are well reproduced by the single-phase monoclinic model, and no systematic misfit or additional Bragg peaks attributable to secondary phases were detected. The refined unit-cell parameters are $a = 8.1222$ Å, $b = 16.0611$ Å, $c = 3.5810$ Å, $\beta = 101.4373°$, and $V = 457.8734$ Å^3, in good agreement with the reported SCOB structure. This analysis confirms that the sample is phase-pure within the detection limits of laboratory XRD and validates the use of this monoclinic SCOB phase as the structural reference for the subsequent thermoluminescence investigation.

3.2. TL filter selection and logarithmic data representation

The thermoluminescence (TL) emission characteristics of $SmCa_4O(BO_3)_3$ were examined using different optical filter configurations to determine the most suitable detection window as shown in Fig. 2. TL measurements were performed using a Lexsyg Smart TL/OSL reader equipped with a bialkali photomultiplier tube (PMT), whose maximum spectral sensitivity lies in the blue–green region. Measurements were carried out employing a TL wideband blue bandpass filter as well as wavelength-selective IRSL/TL filters centered at 365, 410, and 565 nm. Among these, the IRSL/TL–565 nm filter yielded the most intense and well-defined TL signal and was therefore selected for subsequent measurements. Logarithmic data representation was applied where necessary to facilitate comparison of low- and high-intensity regions [28].

3.3. Thermoluminescence glow curve characteristics and preheat optimization

The TL glow curve of $SmCa_4O(BO_3)_3$ recorded at 50 Gy and a heating rate of 2 °C s^{-1} exhibits two main peaks at approximately 80 °C and 240 °C (Fig. 3a). The lower-temperature component is thermally unstable and may influence reproducibility and kinetic evaluation [21,22]. Therefore, a preheating (thermal cleaning) procedure was applied prior to further analysis. The integrated TL area as a function of preheat temperature (Fig. 3b) decreases rapidly below ~120 °C and approaches a quasi-stable regime above ~160–180 °C. Fig. 3c presents the glow curve recorded after applying the optimized preheat at 180 °C for 10 s, where the contribution below ~120 °C is strongly reduced and a single dominant peak remains near 240 °C. Thus, 180 °C was selected as a compromise between suppressing the lower-temperature contribution and maintaining sufficient TL intensity for reliable measurements [29].

3.4. Dose response behavior

The dose response characteristics of SCOB phosphors were investigated by recording thermoluminescence (TL) glow curves over a wide range of β-irradiation doses under optimized experimental conditions. All measurements were performed after applying the optimized preheating treatment (180 °C for 10 s), using a linear heating rate of 2 °C s^{-1} and the IRSL/TL–565 nm detection filter. As illustrated in Fig. 4a, the TL glow curves exhibit a dominant peak centered at approximately 247 °C, whose intensity increases systematically with increasing β dose. Notably, the position of the peak maximum and the overall glow peak shape remain essentially unchanged over the entire investigated dose range. The absence of significant peak broadening or temperature shift with dose suggests that the same trapping–recombination center is responsible for the observed emission and that retrapping effects are relatively weak. Such behavior is commonly regarded as consistent with first-order TL kinetics, where recombination probability is largely independent of trap occupancy and retrapping processes are minimal [22,30].

For a quantitative evaluation of the dose response, the TL signal was characterized using the integrated TL curve area, which provides a more reliable measure than peak height alone, particularly when minor variations in peak shape may occur. Since the TL curve area is less sensitive to peak shape variations and provides a more reliable representation of

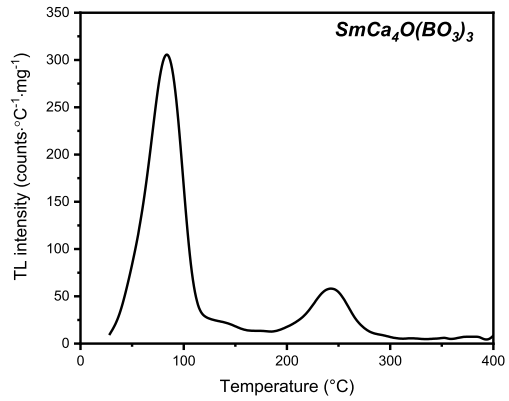

(a)

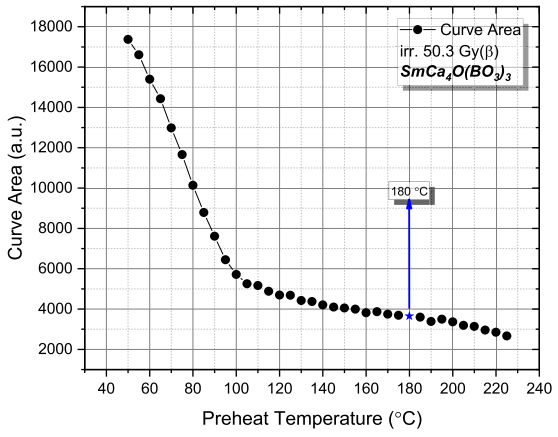

(b)

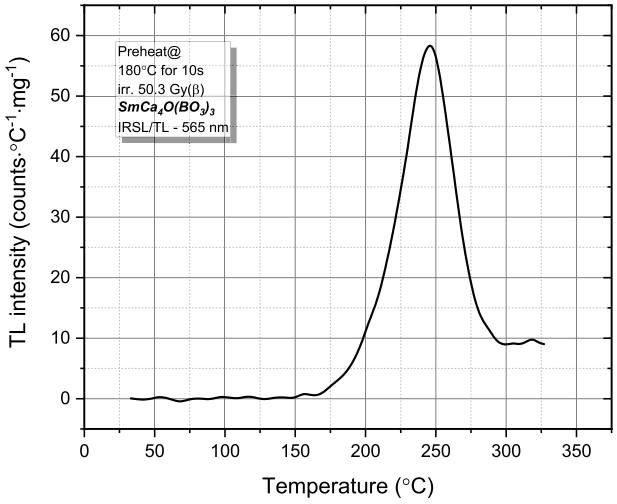

(c)

Fig. 3. (a) TL glow curve of SCOB phosphor recorded after 50.3 Gy β-irradiation at a heating rate of 2 °C s^{-1}, showing two glow peaks at ~82 °C and ~240 °C. (b) Variation of TL curve area as a function of preheat temperature used to determine the optimal preheating condition. (c) TL glow curve of $SmCa_4O(BO_3)_3$ recorded after preheating at 180 °C for 10 s (β-irradiation dose: 50 Gy, heating rate: 2 °C s^{-1}).

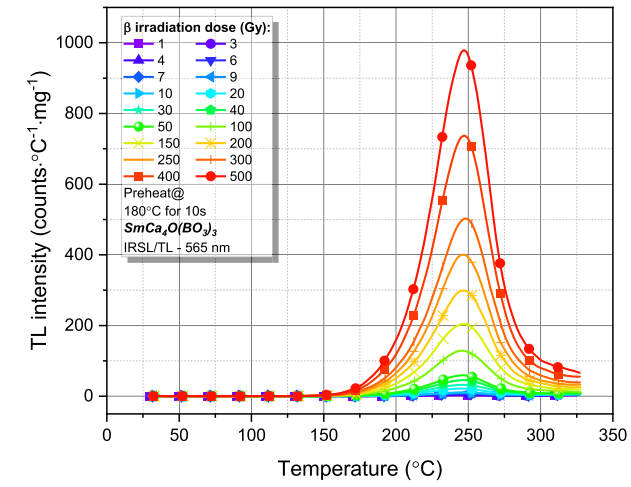

(a)

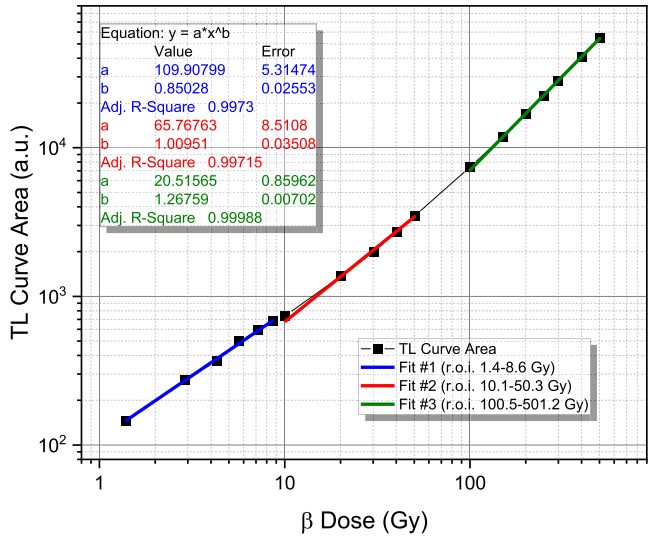

(b)

Fig. 4. (a) TL glow curves of SCOB phosphors recorded at different β-irradiation doses after preheating at 180 °C for 10 s, measured at a heating rate of 2 °C s^{-1} using the IRSL/TL–565 nm filter. (b) Dose response of the integrated TL curve area as a function of β dose plotted on a log–log scale, showing power-law fitting in different dose regions.

the total released charge than peak height, the dose–response analysis in the present study was carried out using the integrated TL curve area. The dependence of the TL curve area on the β-irradiation dose is presented in Fig. 4b on a log–log scale. The experimental data were fitted using a power-law relationship of the form $I = aD^b$, where I represents the TL curve area and D is the absorbed dose.

The log–log representation reveals distinct dose response regimes characterized by different slope values (b). At low doses (1.4-8.6 Gy), a sublinear response ($b < 1$) is observed, which may be attributed to initial trap filling and competition among trapping centers. In the intermediate dose region (10.1-50.3 Gy), the response is approximately linear behavior ($b \approx 1$), indicating efficient filling of the dominant traps without significant saturation effects. At higher doses (100.1 Gy-501.2Gy), a supralinear response ($b > 1$) becomes evident, suggesting the involvement of additional trapping states or enhanced recombination efficiency due to increased carrier population. Similar multi-regime dose response behaviors have been reported in TL materials exhibiting complex trap structures and competing recombination pathways [31–33].

Overall, the observed dose-dependent TL behavior of SCOB phosphors, together with the stability of the main glow peak shape, indicates favorable characteristics for dosimetric applications. The wide dynamic dose range, combined with behavior consistent with first-order kinetics, provides a solid basis for subsequent kinetic analyses and further evaluation of the material's dosimetric performance.

3.5. Reusability and thermal stability

The reusability and thermal stability of the SCOB sample were evaluated through consecutive TL readout cycles performed under identical irradiation and readout conditions. Fig. 5a presents the TL glow curves recorded over ten successive readout cycles following β-irradiation at 50.3 Gy and a preheating treatment at 180 °C for 10 s.

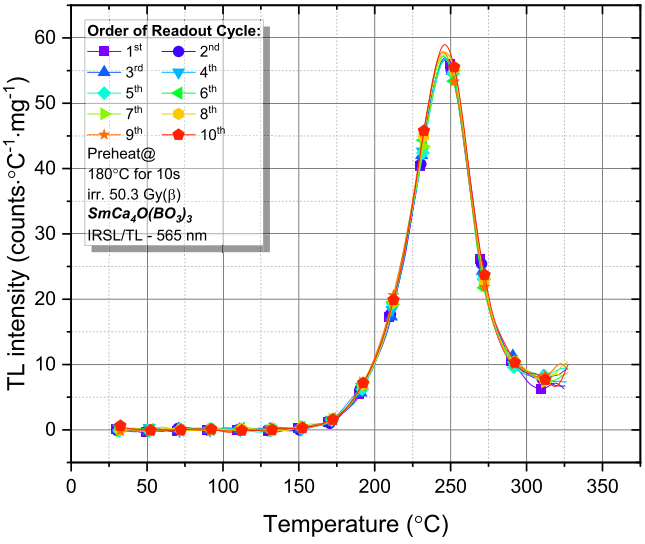

(a)

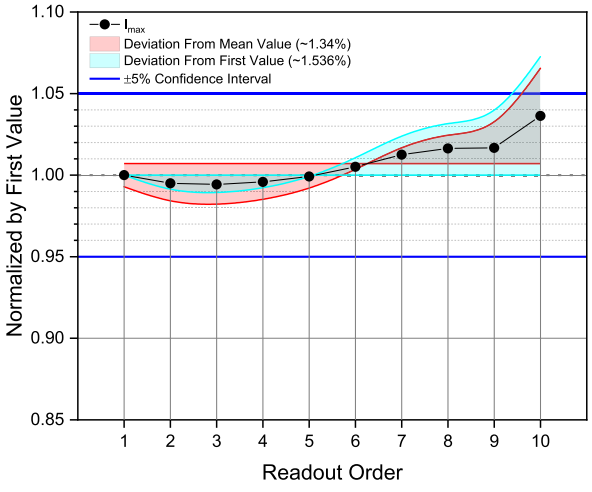

(b)

Fig. 5. (a) TL glow curves of SCOB recorded over ten successive readout cycles after β-irradiation at 50.3 Gy and preheating at 180 °C for 10 s. (b) Normalized maximum TL intensity (I_{max}) versus readout order, showing deviations within ±5%, confirming good reusability and thermal stability of the TL signal.

The glow curves exhibit nearly identical shapes, with no noticeable shift in peak position or emergence of additional low-temperature components, indicating good thermal and structural stability of the trapping centers. To quantitatively assess signal reproducibility, the maximum TL intensity (I_{max}) was normalized to the first readout cycle and plotted as a function of readout order (Fig. 5b). The normalized intensity values remain within a narrow variation band, with deviations from the mean and from the first readout limited to approximately 1.34% and 1.54%, respectively, well within the ±5% confidence interval commonly accepted for TL dosimetric applications. In addition to intensity stability, the corrected peak temperature obtained from ten repeated measurements after the optimized preheating treatment yields $T_m = 247.02 \pm 0.07$ °C (±1σ), corresponding to a relative uncertainty of approximately 0.028%. This small dispersion confirms the thermal stability of the dominant trapping center and the reproducibility of the peak-position determination. The observed stability over repeated readout cycles confirms the robustness of the TL response and demonstrates that the trapping and recombination centers are not significantly altered by successive heating cycles. This high degree of reproducibility provides a reliable experimental basis for the subsequent kinetic analysis of the TL glow curves.

3.6. The minimum detectable dose (MDD) was evaluated using the standard expression

The minimum detectable dose (MDD) was evaluated using commonly used expression

$$D_{LDL} = 3\sigma_{Bkg}\Phi_c \quad (6)$$

where σ_{Bkg} is the standard deviation of the background signal and Φ_C is the calibration factor relating absorbed dose (Gy) to net TL signal intensity. Based on the experimental background statistics and calibration parameters, the MDD was determined to be 11.96 ± 3.60 Gy. This threshold is consistent with the onset of the quasi-linear dose–response region (≈10–50 Gy), indicating that reliable quantitative dosimetry can be performed within the linear regime of the material. Consequently, the obtained detection limit confirms that SCOB is more suitable for medium-to-high dose applications than for low-dose environmental or personal monitoring.

4. Kinetic characterization of thermoluminescence peaks

The kinetic parameters associated with the dominant thermoluminescence (TL) glow peak of SCOB were determined using complementary kinetic approaches. Since the theoretical background of the employed methods has already been presented in Section 2, the present section focuses primarily on the experimental results and their physical interpretation. In order to ensure the reliability of the extracted kinetic parameters, the analysis was initiated using the Variable Heating Rate (VHR) method, which is widely regarded as a robust and model-independent approach for estimating the trap depth. The results obtained from this method provide a consistent basis for subsequent kinetic evaluations.

4.1. Variable heating rate (VHR) analysis

The VHR method was applied by recording TL glow curves at multiple linear heating rates ranging from 0.2 to 5 °C s^{-1}. As expected for thermally activated release processes, the temperature corresponding to the maximum TL intensity (T_m) systematically shifts toward higher temperatures with increasing heating rate. The Hoogenstraaten plots of $\ln(T_m^2/\beta)$ versus $1/(k_B T_m)$ are shown in Fig. 6a using temperature-lag-corrected peak positions. In both cases, a clear linear relationship is observed, indicating that the dominant glow peak can be described by a single effective trap depth within the investigated heating-rate range.

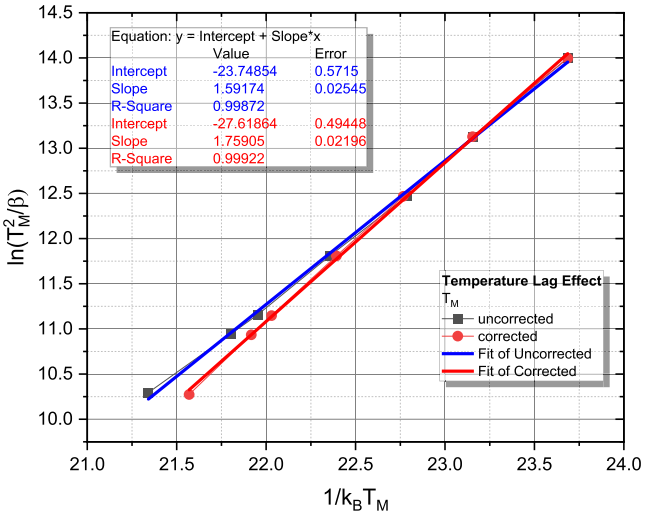

Fig. 6. Hoogenstraaten plots of $\ln(T_m^2/\beta)$ versus $1/(k_B T_m)$ obtained at different heating rates for the main TL peak of SCOB, showing uncorrected and temperature-lag–corrected data along with their linear fits.

From the slope of the corrected plot, a trap depth of 1.75 ± 0.02 eV was obtained. The corresponding frequency factor was calculated to be on the order of 10^{14}–10^{16} s^{-1}.

4.2. T_m–T_{stop} analysis based on preheating temperature

The effect of preheating temperature on the TL glow curve structure of SCOB was investigated using the T_m–T_{stop} method (Fig. 7). As shown in Fig. 7a, increasing the preheating temperature progressively suppresses the low-temperature component, while the high-temperature peak near 247 °C becomes dominant.

Fig. 7b presents the dependence of T_m on T_{stop}. At low preheating temperatures (≤100 °C), T_m increases gradually, indicating the progressive depletion of shallow and thermally unstable traps associated with a quasi-continuous trap distribution. Similar behavior has been reported for borate-based systems by Benavente et al. [34] and Portakal-Uçar et al. [35]. In the intermediate region (~140–225 °C), a plateau is observed where T_m remains nearly constant. This plateau signifies the dominance of a relatively discrete and thermally stable trap family. Within the resolution limits of the T_m–T_{stop} approach, such behavior reflects the prevalence of an energetically clustered trap region rather than a strictly monoenergetic center. Accordingly, the three regions identified in the T_m–T_{stop} curve correspond to broad kinetic regimes.

Fig. 7c shows the variation of activation energy (E_a) with preheating temperature, determined independently using the initial-rise (IR) method applied to partial glow curves. The extracted trap depths increase from ~1.0 to 1.3 eV at low T_{stop} to values exceeding 2.0 eV at higher T_{stop}, indicating the presence of multiple trap families with different thermal stabilities. In contrast to the T_m–T_{stop} representation, which reflects collective kinetic behavior, the E_a–T_{stop} analysis resolves finer energetic substructures within these broader regimes, leading to several distinguishable trap components (Peaks 1–10).

Therefore, the apparent difference between the three kinetic regions observed in Fig. 7b and the larger number of activation-energy clusters in Fig. 7c arises from the different physical quantities and resolution scales probed by the two methods. This behavior is consistent with a hierarchically distributed and energetically non-uniform trap landscape governing the TL response of SCOB.

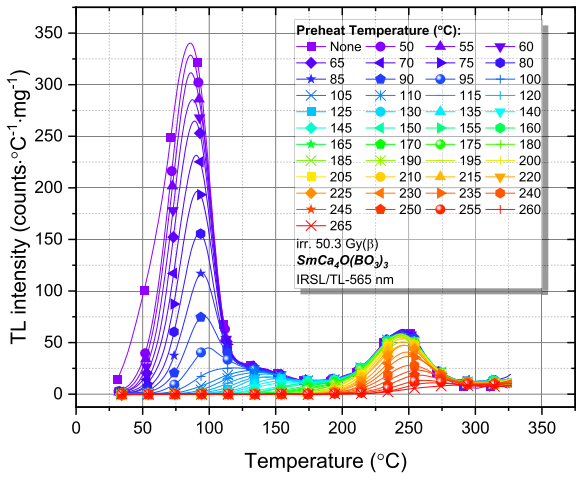

(a)

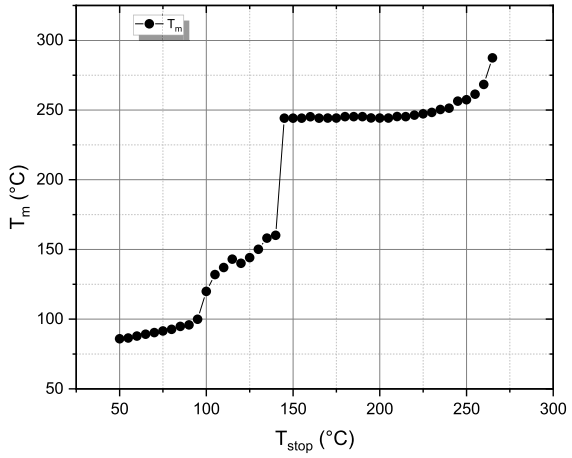

(b)

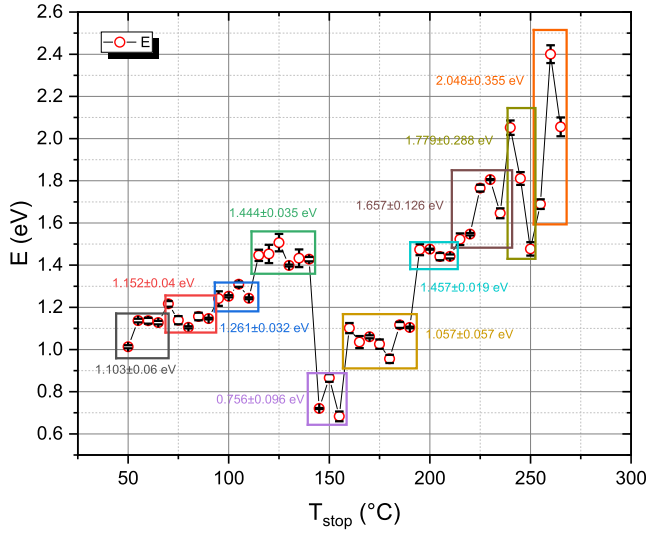

(c)

(caption on next column)

Fig. 7. (a) Evolution of TL glow curves of SCOB phosphor recorded after systematic preheating at different stopping temperatures (T_{stop}). (b) Dependence of the glow peak maximum temperature (T_m) on the stopping (preheating) temperature (T_{stop}), revealing distinct regimes associated with different trapping characteristics, including distributed shallow traps and thermally stable discrete trap levels. (c) Variation of the effective activation energy (E_a) as a function of T_{stop}, obtained from initial rise analysis of partial TL glow curves, illustrating the energy hierarchy of the trapping centers contributing to the thermoluminescence response.

4.3. Glow curve deconvolution analysis and correlation with T_m–T_{stop} results

Computerized glow curve deconvolution (CGCD) was applied to the preheated TL glow curve using a general-order kinetic model in order to resolve overlapping components (Fig. 8). The fitting procedure yielded a satisfactory agreement between experimental and calculated curves (FOM <2.21%), indicating internal consistency of the analysis. It should be emphasized that the numbering of trap groups (Peak 1–Peak 10) is based on the activation energy E extracted as a function of T_{stop} using the initial rise (IR) method applied to partial glow curves, rather than directly from the T_m–T_{stop} trajectory.

As shown in Fig. 7c, the activation energy exhibits clear clustering with increasing T_{stop}, and these clusters define ten distinct trap populations associated with specific preheating intervals. The T_m–T_{stop} curve serves a complementary role by providing qualitative evidence for distributed shallow traps and a thermally stable dominant trap family. These components should not be interpreted as strictly isolated monoenergetic traps but rather as effective trap groups representing energetically clustered states within a non-uniform trap landscape. This interpretation is consistent with the T_m–T_{stop} results, where sloped regions indicate distributed shallow traps and the extended plateau reflects the dominance of a relatively discrete and thermally stable trap family over a broad preheating interval. The kinetic order values ($b = 1.04$–1.25) are consistent with first-order recombination behaviour ($b \approx 1$), indicating limited retrapping effects.

Overall, the combined CGCD and T_m–T_{stop} analyses indicate that the TL response of SCOB is governed by distributed-trap kinetics arising from a hierarchically distributed and interacting trap ensemble rather than a single discrete trapping level, as supported by the segmented T_m–T_{stop} behaviour and the broad activation energy distribution.

It should be noted that these deconvoluted components represent effective trap groups within the general-order kinetic framework rather than strictly isolated monoenergetic traps.

In the SCOB host lattice, the observed TL response arises from intrinsic defect-related trapping and recombination centers rather than from externally introduced activators. The glow curve structure and CGCD analysis reveal multiple effective trap groups with activation energies in the range of approximately 0.86–1.68 eV, indicating the presence of shallow and moderately deep charge trapping states associated with intrinsic lattice defects.

The low-temperature components ($E \approx 0.9$–1.3 eV) correspond to thermally less stable traps that are readily emptied during preheating and therefore mainly act as transient storage centers. In contrast, the dominant mid- and high-temperature emission bands ($E \approx 1.4$–1.7 eV) are attributed to deeper and thermally stable trapping states that serve as the principal charge storage centers responsible for the dosimetric peak.

The kinetic parameters ($b \approx 1$ and frequency factors spanning $\sim 10^{10}$–10^{17} s^{-1}) suggest predominantly localized recombination behavior, with limited retrapping. The broad range of frequency factors reflects the distributed nature of the trapping states rather than a single well-defined trap. Such characteristics are consistent with a semi-localized or distributed-trap scenario, in which recombination occurs through spatially correlated centers rather than via fully delocalized band transport.

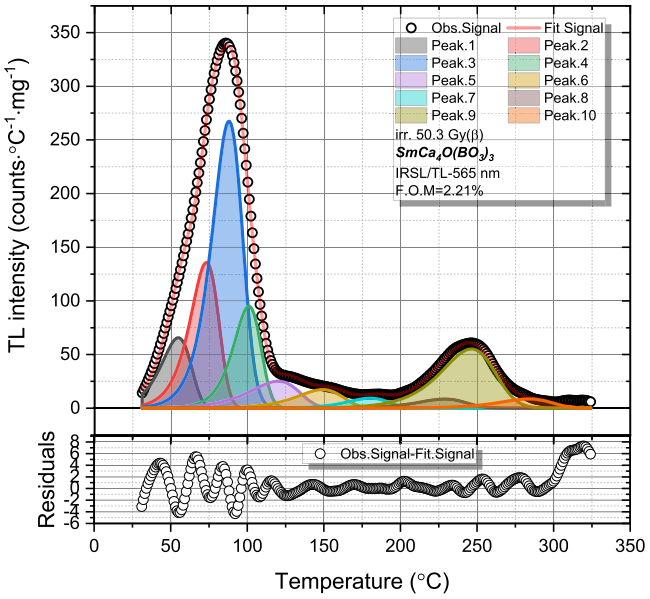

Fig. 8. CGCD analysis of the preheated TL glow curve of SCOB phosphors, illustrating the experimental data, fitted curve, and resolved individual peaks.

Since the material is not intentionally doped beyond its stoichiometric composition, Sm^{3+} ions inherently present in the lattice are considered to act as luminescent recombination centers, while intrinsic defect clusters within the calcium–samarium oxyborate framework provide the ensemble of electron (or hole) trapping sites that govern charge capture, storage, and the observed time-dependent TL enhancement.

4.4. Anomalous time-dependent thermoluminescence enhancement

Fig. 9a shows the evolution of the TL glow curves of the SCOB phosphor as a function of storage time following irradiation under identical experimental conditions. Instead of conventional monotonic fading, the main glow peak exhibits a progressive increase in intensity with increasing storage time. The integrated TL area (Fig. 9b) confirms a delayed and systematic enhancement on a logarithmic time scale.

Such behavior indicates that the post-irradiation defect configuration is not static at ambient conditions. Rather than invoking an increase in the fundamental tunnelling probability over time, the enhancement is more plausibly associated with charge redistribution within a distributed trap ensemble. In complex borate systems, energetically proximate trapping states can enable gradual charge transfer or hopping between traps, thereby modifying recombination competition and radiative efficiency without altering the intrinsic recombination mechanism.

Similar time-dependent luminescence redistribution phenomena have been reported for α-Al_2O_3:C, where charge hopping and trap-to-trap electron transfer between correlated defect states were proposed as governing mechanisms [36]. In addition, sensitivity evolution after repeated irradiation–readout cycles has been documented for α-Al_2O_3:C and α-Al_2O_3:C,Mg [37], where changes in deep-trap occupancy alter charge competition dynamics. Although the present measurements were conducted under identical preheating conditions prior to each readout, a similar redistribution among closely spaced trap levels may contribute to the observed delayed TL enhancement.

While the results clearly demonstrate anomalous time-dependent TL enhancement, further investigation of storage-temperature dependence would be required to distinguish between thermally assisted relaxation and athermal redistribution mechanisms. Therefore, the mechanisms discussed above are proposed as physically plausible interpretations consistent with the distributed-trap structure identified in this study.

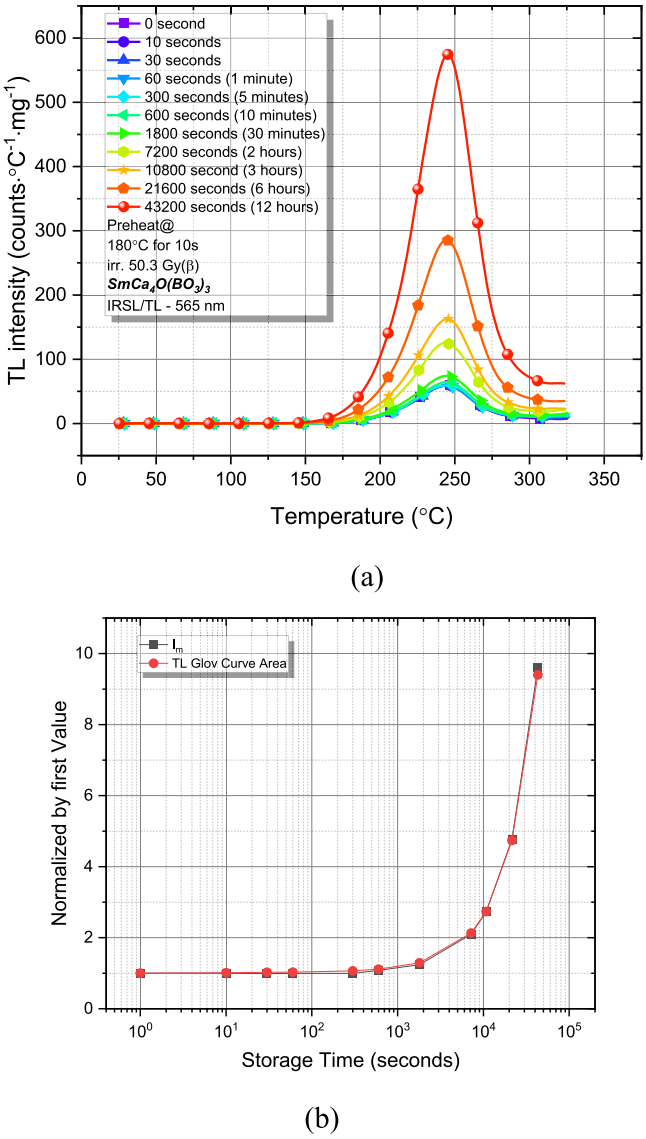

Fig. 9. (a) TL glow curves of the Sm,Ca-doped borate phosphor measured after different storage times, showing a progressive increase of the main glow peak (~220–247 °C). (b) Integrated TL glow-curve area versus storage time (log scale), demonstrating anomalous time-dependent TL enhancement rather than conventional fading.

4.5. Role of Sm^{3+} ions in the trapping and recombination mechanism

In addition to acting as luminescent centers, Sm^{3+} ions may also influence the trapping structure of the SCOB host lattice. Rare-earth ions are known to introduce localized electronic states within the band gap due to their partially filled 4f configuration. Although 4f levels are generally shielded and weakly coupled to the lattice, the incorporation of Sm^{3+} into the Ca^{2+} sites can induce local charge imbalance and associated defect complexes (e.g., oxygen vacancies or borate-related intrinsic defects). These defect–dopant associations may act as effective electron or hole trapping centers.

A similar role of Sm^{3+} ions has been discussed in rare-earth-doped semiconductor systems [38], where Sm^{3+} incorporation modifies the defect landscape and facilitates energy transfer between host-related states and 4f levels. In the present SCOB system, the activation energy of ~1.7 eV obtained from VHR and IR analyses suggests the presence of thermally stable deep traps. While the dominant TL emission is attributed to recombination at Sm^{3+}-related centers, the trapping process

itself is more likely associated with intrinsic or Sm-induced defect complexes rather than isolated 4f states.

Therefore, Sm^{3+} ions in SCOB can be considered to play a dual role:

(i) as recombination centers responsible for characteristic emission, and (ii) indirectly as modifiers of the trapping structure through defect–dopant interactions.

However, based on the first-order kinetic behavior ($b \approx 1$) and the distributed trap analysis (T_m–T_{stop} and CGCD results), the main electron traps appear to be predominantly intrinsic or defect-associated rather than purely Sm^{3+}-centered traps.

5. Conclusions

In this study, the TL properties and trap kinetics of SCOB phosphor were comprehensively investigated using a combined experimental and analytical framework. The material was successfully synthesized via a microwave-assisted sol–gel combustion route, and XRD analysis confirmed the formation of a single-phase monoclinic ceramic structure, providing a stable crystalline framework for thermoluminescence investigations. The initial TL glow curve recorded without preheating revealed the coexistence of pronounced low-temperature peaks and a dominant high-temperature peak, indicating the simultaneous contribution of shallow and deep trapping states. Systematic preheating was therefore employed as an effective thermal filtering strategy to suppress unstable shallow traps and isolate thermally stable trapping centers. Optimization of the preheating conditions led to the selection of 180 °C for 10 s, ensuring reliable and reproducible TL measurements dominated by the main dosimetric peak. Dose–response studies demonstrated a wide dynamic range extending up to 500.8 Gy, with near-linear behavior at low doses and slight supralinearity at higher doses, without evidence of saturation. Reusability tests further confirmed excellent thermal stability and signal reproducibility, with intensity variations well within acceptable limits for TL applications, highlighting the robustness of the ceramic host lattice.

Detailed kinetic analysis using variable heating rate (VHR), initial rise (IR), computerized glow curve deconvolution (CGCD), and T_m–T_{stop} methods revealed a hierarchical and non-uniform trap structure. The TL emission of SCOB is governed by distributed-trap kinetics arising from a hierarchically structured trap ensemble rather than a single discrete trapping level. This interpretation is supported by the segmented T_m–T_{stop} behavior and the broad activation energy range revealed by multi-method analysis. The CGCD components listed in Table 1 should be regarded as effective trap groups within this ensemble rather than strictly isolated monoenergetic traps. An additional and notable outcome of this study is the observation of an anomalous time-dependent thermoluminescence enhancement of the main high-temperature glow peak during post-irradiation storage. Unlike conventional fading behavior, the TL signal increases with storage time, suggesting a redistribution-driven process rather than charge loss. This behavior further supports the presence of complex and spatially correlated defect configurations in the SCOB host lattice.

Overall, the present work provides the first comprehensive thermoluminescence and kinetic characterization of SCOB phosphors using a multi-method analytical approach. The findings demonstrate that intrinsic defect states within this borate-based ceramic host give rise to distributed-trap TL kinetics and a complex trap landscape. These results establish SCOB as a valuable ceramic reference system for understanding trap interactions in rare-earth-containing borates and offer a solid foundation for future dopant-engineered studies and ceramic dosimetric applications.

Table 1
Activation energy (E_a), kinetic order (b), peak temperature (T_m), and frequency factor (s) of the individual TL glow peaks of SCOB phosphors determined by CGCD analysis.

	E_a (eV)	b	T_m (°C)	T_{m1} (°C)	T_{m2} (°C)	μ	s (s^{-1})
1st Peak	1.01	1.08	54.71	41.02	64.37	0.39582	7.27×10^{14}
2nd Peak	1.21	1.12	73.08	60.23	82.35	0.41692	9.53×10^{16}
3rd Peak	1.30	1.25	87.84	74.44	98.13	0.42226	3.22×10^{17}
4th Peak	1.50	1.17	100.84	88.59	109.89	0.41143	4.03×10^{17}
5th Peak	0.86	1.04	119.95	97.09	135.73	0.40379	1.36×10^{10}
6th Peak	1.11	1.11	149.06	128.27	163.96	0.41559	2.54×10^{12}
7th Peak	1.47	1.20	180.11	161.64	193.96	0.42801	3.63×10^{15}
8th Peak	1.52	1.15	228.76	207.09	244.60	0.41261	2.54×10^{14}
9th Peak	1.48	1.18	246.24	222.10	264.17	0.42887	2.29×10^{13}
10th Peak	1.68	1.10	283.73	259.88	300.73	0.40648	1.99×10^{14}

CRediT authorship contribution statement

E. Aymila Cin: Formal analysis, Investigation, Methodology. **K. Bulcar:** Formal analysis, Methodology. **Abeer S. Altowyan:** Formal analysis, Funding acquisition, Investigation, Methodology, Writing – original draft. **M.B. Coban:** Formal analysis, Investigation. **U.H. Kaynar:** Formal analysis, Investigation, Methodology. **H. Muzaffer Sagban:** Investigation, Methodology. **Jabir Hakami:** Conceptualization, Investigation, Methodology. **M. Topaksu:** Investigation, Methodology. **N. Can:** Conceptualization, Supervision, Writing – original draft, Writing – review & editing.

Declaration of competing interest

The authors declare that they have no known competing financial interests or personal relationships that could have appeared to influence the work reported in this paper.

Acknowledgements

The authors acknowledge the Princess Nourah bint Abdulrahman University Researchers Supporting Project (Project No. PNURSP2026R16), Princess Nourah bint Abdulrahman University, Riyadh, Saudi Arabia.

Data availability

Data will be made available on request.

References

[1] S.W.S. McKeever, A Course in Luminescence Measurements and Analyses for Radiation Dosimetry, John Wiley & Sons, 2022.
[2] S.W.S. McKeever, M. Moscovitch, P.D. & Townsend, Thermoluminescence dosimetry materials: properties and uses, Nuclear Technol. Pub. (1995).
[3] V. Chopra, N. El-Faramawy, S.J. Dhoble, Thermoluminescent study of borates for dosimetric applications, in: Phosphor Handb, Elsevier, 2023, pp. 393–415, https://doi.org/10.1016/B978-0-323-90539-8.00013-9.
[4] S. Sangeeta, Sabharwal, thermally stimulated luminescence from alkaline earth borates, J. Lumin. 104 (2003) 267–271, https://doi.org/10.1016/S0022-2313(03)00080-2.
[5] N. El-Faramawy, E.M. Abou Hussein, M. El-Kinawy, Thermoluminescence and structural characterization of crystalline alkali strontium borates, Nucl. Eng. Technol. 57 (2025) 103782, https://doi.org/10.1016/j.net.2025.103782.
[6] J.M. Kalita, Ş. Kaya-Keleş, G.Ö. Çakal, N. Meriç, G.S. Polymeris, Thermoluminescence and optically stimulated luminescence of colemanite-rich borate mineral, J. Lumin. 242 (2022) 118580, https://doi.org/10.1016/j.jlumin.2021.118580.

[7] M.O. Kalinkin, D.A. Akulov, R.M. Abashev, A.I. Surdo, M.V. Kuznetsov, D. G. Kellerman, The role of defects in thermoluminescence of pure and rare-earth-doped magnesium tetraborate phosphor, J. Lumin. 263 (2023) 120119, https://doi.org/10.1016/j.jlumin.2023.120119.

[8] Y. Alajlani, M. Oglakci, A. Barad, U.H. Kaynar, M. Topaksu, A. Canimoglu, N. Can, Anomalous heating rate and kinetic analysis in the thermoluminescence of $GdCa_4O(BO_3)_3$, Radiat. Phys. Chem. 232 (2025) 112614, https://doi.org/10.1016/j.radphyschem.2025.112614.

[9] H.J. Alathlawi, A. Barad, O. Madkhali, G. Souadi, M. Sharahili, J. Hakami, S. Balci, U.H. Kaynar, M. Topaksu, N. Can, Intrinsic thermoluminescence and anomalous heating rate effects in undoped $K_7SrY_2(B_5O_{10})_3$ phosphors: a combined Tm–Tstop and GOK deconvolution study, Appl. Radiat. Isot. 225 (2025) 112092, https://doi.org/10.1016/j.apradiso.2025.112092.

[10] K. Bulcar, S. Akça-Özalp, A.S. Altowyan, U.H. Kaynar, J. Hakami, M. Topaksu, N. Can, Thermoluminescence and kinetic characterization of Sm^{3+}-doped $GdCa_4O(BO_3)_3$ trap distribution, activation energies, and dosimetric potential, Mater. Res. Bull. 192 (2025) 113630, https://doi.org/10.1016/j.materresbull.2025.113630.

[11] Z.S. Khan, N.B. Ingale, S.K. Omanwar, Synthesis and thermoluminescence properties of rare earth-doped $NaMgBO_3$ phosphor, Environ. Sci. Pollut. Res. 23 (2016) 9295–9302, https://doi.org/10.1007/s11356-015-4993-6.

[12] V. Bhatia, D. Kumar, H. Singh, N. Kaur, S.M. Rao, A. Kumar, V. Mehta, S.P. Singh, Effects of Sm^{3+} ions on the structural, optical and thermoluminescence properties of MnKB glass system, J. Phys. Chem. Solid. 161 (2022) 110408, https://doi.org/10.1016/j.jpcs.2021.110408.

[13] G. Souadi, N. Amri, Ü.H. Kaynar, M.B. Coban, O. Madkhali, M. Ayvacikli, N. Can, Novel Sm^{3+} doped $YCa_4O(BO_3)_3$ phosphors: structural and, low and room temperature luminescent insights, Appl. Radiat. Isot. 203 (2024) 111114, https://doi.org/10.1016/j.apradiso.2023.111114.

[14] P.D. Townsend, Y. Wang, Improving interpretations of imperfections in insulating materials for current technologies, Opt. Mater. X 22 (2024) 100327, https://doi.org/10.1016/j.omx.2024.100327.

[15] A.N. Yazici, M. Doğan, V.E. Kafadar, H. Toktamiş, Thermoluminescence of undoped and Ce-doped BaB_4O_7, Nucl. Instrum. Methods Phys. Res., Sect. B 246 (2006) 402–408, https://doi.org/10.1016/j.nimb.2005.12.052.

[16] E. Tekin (Ekdal), A. Ege, T. Karali, P.D. Townsend, M. Prokić, Thermoluminescence studies of thermally treated CaB_4O_7:Dy, Radiat. Meas. 45 (2010) 764–767, https://doi.org/10.1016/j.radmeas.2010.04.009.

[17] Y.T. Arslanlar, K. Bulcar, S. Akça-Özalp, A.S. Altowyan, J. Hakami, U.H. Kaynar, M. Topaksu, N. Can, Energy trap dynamics and thermoluminescent behaviour of Sm^{3+}-doped $LaCa_4O(BO_3)_3$ under variable conditions, J. Lumin. 283 (2025) 121263, https://doi.org/10.1016/j.jlumin.2025.121263.

[18] W. Hoogensraaten, Electron traps in ZnS phosphorus, philips res, Rep. 13 (1958) 515–693.

[19] R. Chen, V. Pagonis, Thermally and Optically Stimulated Luminescence, Wiley, 2011, https://doi.org/10.1002/9781119993766.

[20] G. Kitis, J.W.N. Tuyn, A simple method to correct for the temperature lag in TL glow-curve measurements, J. Phys. D Appl. Phys. 31 (1998) 2065–2073, https://doi.org/10.1088/0022-3727/31/16/017.

[21] S.W.S. McKeever, Thermoluminescence of solids, in: Cambridge Solid State Science Series. Xiv, 376, Cambridge University Press, Cambridge, London, New York, New Rochelle, Melbourne, Sydney, 1986, pp. 471–472, https://doi.org/10.1017/S0016756800033756. Price £40.00, U.S. $69.50. ISBN 0 521 24520 6., Geol. Mag. 123.

[22] R. Chen, S.W.S. McKeever, Theory of Thermoluminescence and Related Phenomena, World Scientific, 1997, https://doi.org/10.1142/2781.

[23] G.F.J. Garlick, A.F. Gibson, The electron trap mechanism of luminescence in sulphide and silicate phosphors, Proc. Phys. Soc. 60 (1948) 574–590, https://doi.org/10.1088/0959-5309/60/6/308.

[24] J.M. G mez Ros, G. Kitis, Computerised glow curve deconvolution using general and mixed order kinetics, Radiat. Protect. Dosim. 101 (2002) 47–52, https://doi.org/10.1093/oxfordjournals.rpd.a006029.

[25] H.G. Balian, N.W. Eddy, Figure-of-merit (FOM), an improved criterion over the normalized chi-squared test for assessing goodness-of-fit of gamma-ray spectral peaks, Nucl. Instrum. Methods 145 (1977) 389–395, https://doi.org/10.1016/0029-554X(77)90437-2.

[26] S.K. Misra, N.W. Eddy, IFOM, a formula for universal assessment of goodness-of-fit of gamma ray spectra, Nucl. Instrum. Methods 166 (1979) 537–540, https://doi.org/10.1016/0029-554X(79)90546-9.

[27] J. Peng, Z. Dong, F. Han, Tgcd: an R package for analyzing thermoluminescence glow curves, SoftwareX 5 (2016) 112–120, https://doi.org/10.1016/j.softx.2016.06.001.

[28] N. Can, P.D. Townsend, Y. Wang, Analytical benefits from logarithmic displays of luminescence sensitivity, Vacuum 238 (2025) 114273, https://doi.org/10.1016/j.vacuum.2025.114273.

[29] R. Kameshwaran, K. Ganesh Kumar, K. Aravinth, A. Raja, K. Ramachandran, D. O. Annalakshmi, P. Balaji Bhargav, S. Mullai Venthan, K. Gokulkannan, Photoluminescence and thermoluminescence behaviour of Pr^{3+} doped sodium bismuth phosphate phosphors, J. Alloys Compd. 1034 (2025) 181330, https://doi.org/10.1016/j.jallcom.2025.181330.

[30] G. Kitis, J.M. Gomez-Ros, J.W.N. Tuyn, Thermoluminescence glow-curve deconvolution functions for first, second and general orders of kinetics, J. Phys. D Appl. Phys. 31 (1998) 2636–2641, https://doi.org/10.1088/0022-3727/31/19/037.

[31] Y.S. Horowitz, D. Yossian, Computerised glow curve deconvolution: application to thermoluminescence dosimetry, Radiat. Protect. Dosim. 60 (1995) 3, https://doi.org/10.1093/oxfordjournals.rpd.a082702.

[32] A.J.J. Bos, Theory of thermoluminescence, Radiat. Meas. 41 (2006) S45–S56, https://doi.org/10.1016/j.radmeas.2007.01.003.

[33] V. Kortov, Materials for thermoluminescent dosimetry: current status and future trends, Radiat. Meas. 42 (2007) 576–581, https://doi.org/10.1016/j.radmeas.2007.02.067.

[34] J.F. Benavente, J.M. Gómez-Ros, V. Correcher, Characterization of the thermoluminescence glow curve of $Li_2B_4O_7$:Cu,Ag, Radiat. Meas. 137 (2020) 106427, https://doi.org/10.1016/j.radmeas.2020.106427.

[35] Z.G. Portakal-Uçar, M. Oglakci, V. Correcher, M. Sonsuz, N. Can, Y.Z. Halefoglu, M. Topaksu, A thermoluminescence study of Tb^{3+} doped LaB_3O_6: dosimetric characteristics and kinetic parameters, J. Lumin. 253 (2023) 119493, https://doi.org/10.1016/j.jlumin.2022.119493.

[36] J.M. Kalita, M.L. Chithambo, On the sensitivity of thermally and optically stimulated luminescence of α-Al_2O_3:C and α-Al_2O_3:C,Mg, Radiat. Meas. 99 (2017) 18–24, https://doi.org/10.1016/j.radmeas.2017.03.006.

[37] J.M. Kalita, M.L. Chithambo, A comparative study of the dosimetric features of α-Al_2O_3:C,Mg and α-Al2O3:C, Radiat. Protect. Dosim. 177 (2017) 261–271, https://doi.org/10.1093/rpd/ncx039.

[38] N.D. Vinh, P.M. Tan, P.V. Do, S. Bharti, V.X. Hoa, N.T. Hien, N.T. Luyen, N.X. Ca, Effect of dopant concentration and the role of ZnS shell on optical properties of Sm^{3+} doped CdS quantum dots, RSC Adv. 11 (2021) 7961–7971, https://doi.org/10.1039/D0RA08056J.